PROC. OF JSCE
No. 326, October 1982

NUMERICAL ANALYSIS ON THE DYNAMIC RESPONSE OF THREE-DIMENSIONAL, FREE-FLOATING STRUCTURE

*By Wataru KIOKA**

1. INTRODUCTION

In recent years increasing attention has been given to the development of numerical methods related to the wave interaction with a large structure of arbitrary shape. Such wave-structure interaction occurs either as a radiation (forced-motion) problem or as a diffraction problem. For many structures in the ocean, the boundary-value problem arising from both cases must be solved in three dimensions, and the presence of the ocean bottom must be included in the analysis.

Among the existing methods, the Green-function method (the source-distribution method) achieves the most computational efficiency in applications to the present problem. Here we are primarily concerned with the details of the behavior of the field variables near and on the body surface while assuming a smooth variation of the field variables within the fluid domain. The finite-element variational method[1),2)], however, requires modelling the whole fluid domain and thus a large amount of computation. The integral-equation method[3)], which works with the entire fluid boundary but with a simple kernel, involves a full matrix (the band-width associated with the matrix is large). Moreover, for these two methods it is crucial to construct the numerical radiation boundary that reduces the exact problem defined in the infinite domain to an approximate problem in a finite domain. The method of continuation of velocity potentials proposed by Ijima et al.[4)] is limited to the two-dimensionalized problem.

Applications of the Green-function method to the wave-structure problem in three dimensions were intensively made by Garrison et al.[5)~7)] who treated the response of a sphere and a vertical circular cylinder floating in water of finite depth as well as the forces on a hemispherical body and an oil tank configuration bottom-mounted in water of finite depth. However, the method of Garrison et al. has several limitations in applications to arbitrary shape, one of which is that the faceted source surface necessarily has small openings. Without having a large number of elements, this leaking behavior of the sources leads to inaccurate results.

The aim of this paper is to develop a procedure for evaluating the hydrodynamic forces due to the wave-body interaction which does not have these limitations and, specifically, a procedure which is well suited for the three-dimensional bodies of arbitrary shape, both submerged and floating in the range of water depths and frequencies of interest for large structures. The analysis deals with the hydrodynamic forces exerted on the body oscillating in its six degrees of freedom as well as the diffraction forces on the body held fixed. The computed forces are used in conjunction with the equation of motion of the floating body to determine the dynamic response of several free-floating bodies. The cross-coupling forces associated with oscillation of the body are included in the analysis. The validity of the numerical results is examined for the cases of a free-floating vertical circular cylinder by comparing with experimental data. It should be mentioned here that the virtual plate-loaded scheme proposed by Hino and Miyanaga[8)] presents an alternate efficient means of computation, but applications of their method to the surface boundary of complex shape may not be straightforward. Although the method proposed hereinafter is based on a finite-element technique, properly handling integrals of the kernel function over the faceted surface the method does not require a large investment in computer time.

2. FORMULATION OF THE PROBLEM

(1) Linearized Boundary-Value Problems

Consider a rigid body of arbitrary shape which has a characteristic linear dimension, a (such as the radius of a sphere), floating in an inviscid,

* Member of JSCE, Research Associate, Department of Civil Engineering, Nagoya Institute of Technology

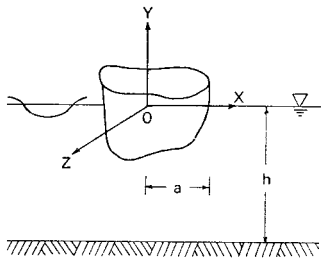

Fig. 1 Definition Schematic.

incompressible fluid of constant depth, h, as shown in **Fig. 1**. The body is assumed to be finite in extent and smooth, so that its normal vector is a continuous function. Otherwise, no restrictions on the geometry of the body are necessary. The body is considered to oscillate harmonically about an inertial coordinate system $0xyz$, with $0y$ pointing upwards and $x0z$ being the undisturbed free surface. Furthermore, the motion of the body and the fluid is assumed to be small, so that we can linearize the boundary condition on the body and the free surface condition. With such assumptions the following boundary-value problem can be formulated in terms of the velocity potential Φ describing the fluid motion.

Let ω be the angular frequency of oscillation when the transient motion disappears. The time and spatial decomposition of Φ may be given by

$$\Phi(x, y, z, t)=Re[\phi_0 e^{-i\omega t}+\phi_7 e^{-i\omega t}+\sum_{m=1}^{6}\phi_m\xi_m(t)], \quad \cdots\cdots(1)$$

where $\phi_0 e^{-i\omega t}$ is the incident wave potential and $\phi_7 e^{-i\omega t}$ the scattering potential for the restrained body. The last term $\phi_m\xi_m$, $m=1, 2, \ldots 6$, represents the velocity potential of the body oscillating in its six degrees of freedom, with $\xi_m(t)$ being the complex-valued time-harmonic amplitude of the body motion. The subscript $m=1, 2, 3$ denotes oscillation in the x, y, z directions (surge, heave and sway), respectively, and $m=4, 5, 6$ denotes angular oscillation about x, y, z axes (roll, yaw and pitch), respectively. The velocity potential of the incident wave propagating in the positive x-direction is known from linear theory, and ϕ_0 is given by

$$\phi_0=-\frac{ig\eta^0}{\omega}\frac{\cosh k(h+y)}{\cosh kh}e^{ikx} \quad \cdots\cdots(2)$$

where η^0 is the wave amplitude and g the acceleration of gravity. The wave number is defined as $k=2\pi/L$ where L denotes the wavelength and is related to the frequency of the wave by dispersion relationship:

$$\frac{\omega^2}{g}=k\tanh(kh). \quad \cdots\cdots(3)$$

The potential functions ϕ_m, $m=0, 1, 2, \ldots 7$, must satisfy:

$$\nabla^2\phi_m=0 \quad \text{throughout the fluid domain,} \quad \cdots\cdots(4)$$

$$\frac{\partial\phi_m}{\partial y}-\nu\phi_m=0, \quad \nu=\frac{\omega^2}{g} \quad \text{on } y=0, \quad \cdots\cdots(5)$$

$$\frac{\partial\phi_m}{\partial y}=0 \quad \text{on } y=-h. \quad \cdots(6)$$

In addition, ϕ_m, $m=1, 2, \ldots 7$ must satisfy the normal boundary condition on the wetted surface of the body at its equilibrium position, S:

$$\frac{\partial\phi_m}{\partial n}=f_m(s), \quad \cdots\cdots(7)$$

where $\partial/\partial n$ is the normal derivative in the direction of the unit inward normal $\boldsymbol{n}$ of the body, and the function $f_m(s)$ is prescribed by

$$f_m(s)=n_m, \quad m=1, 2, \cdots 6, \quad \cdots\cdots(8)$$
$$f_7(s)=-\partial\phi_0/\partial n$$

with $(n_1, n_2, n_3)=\boldsymbol{n}$, $(n_4, n_5, n_6)=(\boldsymbol{r}-\boldsymbol{r}_c)\times\boldsymbol{n}$. Here $\boldsymbol{r}$ is the position vector $\boldsymbol{r}=(x, y, z)$ and $\boldsymbol{r}_c$ the location of the center of rotation. Furthermore, in order to make the problems well-posed, ϕ_m, $m=1, 2, \ldots 7$, must satisfy a radiation condition guaranteeing that the waves are outgoing and have proper amplitude behavior at infinity. If the fluid is of constant depth and the body is bounded in extent, the sufficient radiation condition is given by the general form

$$\lim_{R\to\infty}\sqrt{R}\left[\frac{\partial\phi_m}{\partial R}-ik\phi_m\right]=0, \quad \cdots\cdots(9)$$

where

$$R=(x^2+z^2)^{1/2}$$

The boundary-value problems for ϕ_m, $m=1, 2, \ldots 7$, specified in Eqs. (4)~(9) are all identical except for the boundary conditions prescribed by the functions $f_m(s)$. This allows us to solve the problems for oscillation in the six degrees of freedom and scattering of the incident wave, simultaneously.

(2) Hydrodynamic Forces and Equations of Motion

The forces and moments acting on the immersed surface of the body can be obtained by integrating the fluid pressure P over the surface S. The pressure P is given by the linearized form of Bernoulli's equation

$$P(x, y, z, t)=-\rho\frac{\partial\Phi}{\partial t}-\rho gy, \quad \cdots\cdots(10)$$

where ρ is the mass density of surrounding fluid. Our task here is to evaluate the first term in Eq.

(10) for the hydrodynamic force $\boldsymbol{F}$ and moment $\boldsymbol{M}$. Substituting for Φ from Eq. (1), we obtain

$$\begin{pmatrix}\boldsymbol{F}(t)\\ \boldsymbol{M}(t)\end{pmatrix}=-\rho Re\left[\sum_{m=1}^{6}\ddot{\xi}_m\iint_S\phi_m\begin{pmatrix}\boldsymbol{n}\\ \boldsymbol{r}\times\boldsymbol{n}\end{pmatrix}dS\right]-\rho Re\left[i\omega e^{-i\omega t}\iint_S(\phi_0+\phi_7)\begin{pmatrix}\boldsymbol{n}\\ \boldsymbol{r}\times\boldsymbol{n}\end{pmatrix}dS\right] \quad \cdots\cdots(11)$$

The resulting force and moment from the first integral in Eq. (11) are generally resolved into components in phase with the acceleration of the body and other components in phase with the velocity of the body:

$$M_{ij}+iN_{ij}/\omega=\rho\iint_S\phi_j f_i(s)dS\,,\quad i,j=1,2,\cdots 6, \quad \cdots\cdots(12)$$

where the index i denotes the direction of the force or moment and j indicates the mode of oscillation. The M_{ij} and N_{ij} represent added-mass and damping coefficients, respectively. The nondimensional added-mass and damping coefficients are defined by

$$\left.\begin{aligned}\bar{M}_{ij}=M_{ij}/\rho a^3\,,\quad \bar{N}_{ij}=N_{ij}/\rho\omega a^3\,,\\ i=1,2,3,\ j=1,2,\cdots 6,\\ \bar{M}_{ij}=M_{ij}/\rho a^4\,,\quad \bar{N}_{ij}=N_{ij}/\rho\omega a^4\,,\\ i=4,5,6,\ j=1,2,\cdots 6.\end{aligned}\right\}\quad\cdots\cdots(13)$$

The second term in Eq. (11) is the exciting force and moment F_e, and their components are nondimensionalized as

$$\left.\begin{aligned}\bar{F}_{ei}=F_{ei}/\rho g a^2\eta^0\,,\quad i=1,2,3\,,\\ \bar{F}_{ei}=F_{ei}/\rho g a^3\eta^0\,,\quad i=4,5,6\,.\end{aligned}\right\}\quad\cdots\cdots(14)$$

The nondimensional force and moment components can be further expressed in the form

$$\bar{F}_{ei}=Re[C_i e^{i\delta i}e^{-i\omega t}],\quad i=1,2,\cdots 6, \quad\cdots\cdots(15)$$

where C_i represents the amplitude of $\bar{F}_{ei}$ and δ_i denotes its phase angle with respect to the phase of the incident wave.

The set of equations of the body motion $\xi_j(t)$, $j=1,2,\ldots,6$, is well known and is simply reproduced here.

$$(m_{ij}+M_{ij})\ddot{\xi}_j+N_{ij}\dot{\xi}_j+c_{ij}\xi_j=F_{ei}\,,\quad i=1,2,\cdots 6, \quad\cdots\cdots(16)$$

The mass matrix elements m_{ij} and hydrostatic stiffness matrix elements c_{ij} are given in the conventional forms, for instance, by Wehausen[9] and the nonzero elements can be readily derived for a given body. Using the nondimensional coefficients introduced above and substituting further the assumed form $\xi_j=Re[X_j e^{i\psi j}e^{-i\omega t}]$, Eq. (16) yields a complex matrix equation

$$[-\nu(\bar{m}_{ij}+\bar{M}_{ij})-i\nu\bar{N}_{ij}+\bar{c}_{ij}](X_j/\eta^0)e^{i\psi j}=C_i e^{i\delta i} \quad\cdots\cdots(17)$$

where ψ_j denotes the phase angle of the motion with respect to the phase of the incident wave, and nonzero coefficients m_{ij} and c_{ij} are nondimensionalized as $\bar{m}_{ii}=m_{ii}/\rho a^3$, $i=1,2,3$, $\bar{m}_{ij}=m_{ij}/\rho a^5$, $i,j=4,5,6$, $\bar{c}_{22}=c_{22}/a^2$, $\bar{c}_{24}=\bar{c}_{42}=c_{24}/a^3$, $\bar{c}_{26}=\bar{c}_{62}=c_{26}/a^3$, $\bar{c}_{44}=c_{44}/a^4$, $\bar{c}_{46}=\bar{c}_{64}=c_{46}/a^4$, and $\bar{c}_{66}=c_{66}/a^4$. This is a set of six linear equations, which can be solved for the amplitude ratio X_j/η^0 and the phase lag by matrix-inversion procedure.

3. SOURCE-DISTRIBUTION METHOD

To simplify the notation, henceforth, the subscript m of the potentials will be omitted with understanding that ϕ will always depend on m.

In 1950, John[10] showed that for a body of general shape the potential functions associated with the problem can be obtained by distributing a point wave source of unit strength, G, over the surface of the body according to the source strength function σ:

$$\phi(x,y,z)=\iint_S\sigma(\xi,\eta,\zeta)G(x,y,z;\xi,\eta,\zeta)dS\,, \quad\cdots\cdots(18)$$

where (ξ,η,ζ) denotes the coordinates of a point on the immersed surface of the body S. This representation of ϕ is unique. The potential for the unit sources G, that is the Green function for the problem, is generally given in the form

$$G(x,y,z;\xi,\eta,\zeta)=1/r+H(x,y,z;\xi,\eta,\zeta)\,, \quad\cdots\cdots(19)$$

where

$$r=[(x-\xi)^2+(y-\eta)^2+(z-\zeta)^2]^{1/2}\,.$$

The singularity $1/r$ is a particular solution of the Laplace equation (4) while H is a regular function satisfying Eq. (4). This harmonic function H can be so constructed that G satisfies all the boundary conditions, except the boundary condition on the body surface given by Eq. (7). The form of ϕ given by Eq. (18) automatically satisfies Eqs. (5), (6) and (9) as G itself satisfies these equations. The source strength function σ must be determined in such a way that ϕ satisfies the normal boundary condition on the body surface (i.e., the Neumann condition) as given by Eq. (7). This results in the following well-known Fredholm integral equation of the second kind over the surface S:

$$-2\pi\sigma(x,y,z)+\iint_S\sigma(\xi,\eta,\zeta)\cdot\frac{\partial G}{\partial n}(x,y,z;\xi,\eta,\zeta)dS=f(s)\,, \quad\cdots\cdots(20)$$

where $-2\pi\sigma$ is the contribution of the local source strength to the local normal velocity. Once

this integral equation is solved for σ, the potential at any point can be determined from Eq. (18) by evaluating the surface integral. Then the evaluation of all other physical quantities such as forces and moments is straightforward.

The Green function defined in Eq. (19) is given by Wehausen and Laitone[11] as

$$G(x,y,z;\xi,\eta,\zeta)=1/r+1/r' +G^*(x,y,z;\xi,\eta,\zeta), \cdots(21)$$

where

$$G^*=2P.V. \cdot \int_0^\infty \frac{(\mu+\nu)e^{-\mu h}\cosh\mu(\eta+h)\cosh\mu(y+h)}{\mu\sinh\mu h-\nu\cosh\mu h} \cdot J_0(\mu R)d\mu +i\frac{2\pi(k^2-\nu^2)\cosh k(\eta+h)\cosh k(y+h)}{k^2h-\nu^2h+\nu} \cdot J_0(kR),$$

$$r'=[(x-\xi)^2+(y+2h+\eta)^2+(z-\zeta)^2]^{1/2},$$

$$R=[(x-\xi)^2+(z-\zeta)^2]^{1/2}.$$

Here J_0 is the Bessel function of the first kind of order zero and $P.V.$ indicates a principal-value integral. The first two terms of Eq. (21) are seen to be the potentials of $1/r$-type point sources; one located at the source point and one at its image in the bottom boundary. The infinite integral term and imaginary term are necessary to satisfy the free-surface condition and the radiation condition.

4. NUMERICAL SOLUTION

The approach to the numerical solution of the integral equation (20) requires an approximate representation of the body surface and an approximate evaluation of the relevant integral. In the customarily used method (e.g., the method of Garrison et al.), the body surface was approximated by a number of quadrilateral elements and a surface source of constant strength was distributed over each element. The Neumann boundary condition was then applied at the center of each element. For an arbitrary body, however, all four corners cannot match the corners of adjacent elements. If the center of each element is arranged to lie exactly on the body surface, some parts of some elements are outside of the actual body. Moreover, the resulting potential is discontinuous across the element since the source strength jumps stepwise at the element boundary. Thus physical quantities such as pressures and velocities on the body surface can be safely evaluated only at the centers of each element.

The problems mentioned above may be eliminated by the use of triangular elements with a continuous source-strength distribution. The approach proposed here can be regarded as an extention of the numerical method of Webster[12] developed for computing the potential flow about an arbitrary body in an unbounded fluid.

(1) Triangular Source Element

In deriving the basic equations of the method it is convenient to assume that a triangular element lies in the $\hat{x}\hat{y}$-plane as shown in **Fig. 2.** The local coordinate system $0\hat{x}\hat{y}\hat{z}$ is chosen so that one side of the triangle lies on the $\hat{x}$ axis and the remaining vertex lies on the $\hat{y}$ axis. The $\hat{x}\hat{y}$ coordinates of the three corner points defining the triangle are denoted by $(\hat{a}, 0)$, $(\hat{d}, 0)$ and $(0, \hat{b})$.

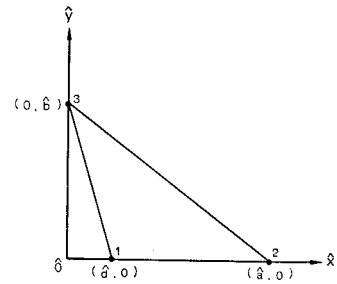

Fig. 2 Triangular Source Element.

If the Green function is expressed in the local coordinate system, the potential induced by the triangular source element at a general point is given from Eq. (18) as

$$\phi(\hat{x},\hat{y},\hat{z})=\iint_A \sigma(\hat{\xi},\hat{\eta})G(\hat{x},\hat{y},\hat{z};\hat{\xi},\hat{\eta})d\hat{\xi}d\hat{\eta}, \cdots(22)$$

where the range of the integration is the area A of the triangle. The source strength function is assumed to be a linear function of $(\hat{\xi}, \hat{\eta})$ as

$$\sigma(\hat{\xi},\hat{\eta})=\alpha+\beta\hat{\xi}+\gamma\hat{\eta}. \cdots(23)$$

The coefficients α, β and γ are uniquely determined by using the source strength at each vertex:

$$\sigma(\hat{a},0)=\sigma_a, \quad \sigma(0,\hat{b})=\sigma_b, \quad \sigma(\hat{d},0)=\sigma_d. \cdots(24)$$

Eq. (22) is then rewritten in the form

$$\phi(\hat{x},\hat{y},\hat{z})=\sigma_a\phi_a(\hat{x},\hat{y},\hat{z})+\sigma_b\phi_b(\hat{x},\hat{y},\hat{z}) +\sigma_d\phi_d(\hat{x},\hat{y},\hat{z}), \cdots(25)$$

where

$$\phi_a=\iint_A d\hat{\xi}d\hat{\eta}(-\hat{b}\hat{d}+\hat{b}\hat{\xi}+\hat{d}\hat{\eta})G/\hat{b}(\hat{a}-\hat{d}),$$

$$\phi_b=\iint_A d\hat{\xi}d\hat{\eta}(\hat{\eta}/\hat{b})G\,,$$

$$\phi_d=\iint_A d\hat{\xi}d\hat{\eta}(\hat{a}\hat{b}-\hat{b}\hat{\xi}-\hat{a}\hat{\eta})G/\hat{b}(\hat{a}-\hat{d})\,.$$

The induced velocity vector $\boldsymbol{v}$ due to the triangular source element is given by

$$\boldsymbol{v}=\sigma_a \underbrace{\text{grad}\,\phi_a}+\sigma_b \underbrace{\text{grad}\,\phi_b}+\sigma_d \underbrace{\text{grad}\,\phi_d}\,. \quad \cdots\cdots(26)$$

The computation of the potential functions, ϕ_a, ϕ_b and ϕ_d, and their derivatives are sufficiently complicated that it is worthwhile to consider the contribution of each of the terms in the Green function separately. The first term in the Green function, $1/r$, becomes singular as the field point approaches the source point while the others are regular everywhere below $y=0$. The first two terms, $1/r$ and $1/r'$, vary rapidly near the source point. On the other hand, the frequency-dependent part, G^*, varies slowly and oscillates with a given wavelength.

The use of a linear variation of the source strength removes a difficulty in carrying out the analytical integration due to the singular behavior of $1/r$. That is, an assumption of linearly varying source-strength function yields the smooth behavior of the potential functions induced by the $1/r$ source. The potential functions which are expressed as Eq. (25) and their derivatives can be given in terms of elementary functions for a triangular element of general shape, without using an image element such as a inner circular element. The resulting equations are shown in Appendix. These basic equations can be approximated by a set of discrete sources when the field point is far from the source element. This can be accomplished by expanding the function $1/r$ in a Taylor series about $(\hat{\xi}, \hat{\eta})$. For a large distance from the source element, the potential functions yield

$$\left.\begin{aligned}\phi_a{}^r&\approx(A/3)[(\hat{x}-\hat{\xi}_a)^2+(\hat{y}-\hat{\eta}_a)^2+\hat{z}^2]^{-1/2}\,,\\ \phi_b{}^r&\approx(A/3)[(\hat{x}-\hat{\xi}_b)^2+(\hat{y}-\hat{\eta}_b)^2+\hat{z}^2]^{-1/2}\,,\\ \phi_d{}^r&\approx(A/3)[\hat{x}-\hat{\xi}_d)^2+(\hat{y}-\hat{\eta}_d)^2+\hat{z}^2]^{-1/2}\,,\end{aligned}\right\} \quad \cdots\cdots(27)$$

where the three discrete source points are given by

$$(\hat{\xi}_a, \hat{\eta}_a)=(\hat{a}/2+\hat{d}/4, \hat{b}/4)\,,$$
$$(\hat{\xi}_b, \hat{\eta}_b)=(\hat{a}/4+\hat{d}/4, \hat{b}/2)\,,$$
$$(\hat{\xi}_d, \hat{\eta}_d)=(\hat{a}/4+\hat{d}/2, \hat{b}/4)\,.$$

It was found that the error in the potentials computed from Eq. (27) is less than 0.1 percent if the ratio of the distance between a particular field point and the origin of the local coordinate system to the length of the largest side of the triangle is larger than 5.0[13].

Carrying out the analytical integration of G^*, however, is not possible for a triangular element of general shape. Because of the slowly varying nature of G^*, an appropriate approximation is to evaluate the integrand G^* at the three discrete source points defined in Eq. (27) and multiply by $A/3$. The validity of these approximate integrals is ensured if one keeps each element small enough compared with a wavelength.

Consequently, the potential induced by the triangular source element is expressed in the following form:

$$\begin{aligned}\phi(\hat{x}, \hat{y}, \hat{z})=\sigma_a[&\phi_a{}^r+\phi_a{}^{r'}\\ &+(A/3)G^*(\hat{x}, \hat{y}, \hat{z}; \hat{\xi}_a, \hat{\eta}_a)]\\ &+\sigma_b[\phi_b{}^r+\phi_b{}^{r'}+(A/3)\\ &\cdot G^*(\hat{x}, \hat{y}, \hat{z}; \hat{\xi}_b, \hat{\eta}_b)]+\sigma_d[\phi_d{}^r+\phi_d{}^{r'}\\ &+(A/3)G^*(\hat{x}, \hat{y}, \hat{z}; \hat{\xi}_d, \hat{\eta}_d)]\,, \quad \cdots(28)\end{aligned}$$

where the induced potentials, $\phi_a{}^{r'}$, $\phi_b{}^{r'}$ and $\phi_d{}^{r'}$, due to the second term in Eq. (21), $1/r'$, can be readily evaluated by the formulas given in Appendix if r is replaced by r'.

(2) Numerical Procedure

We assume here that the potentials and velocities computed in the local coordinate system are transformed to those in the global coordinate system $0xyz$.

Let us approximate the body surface by K elements as shown schematically in **Fig. 3**. The potential due to these K elements is expressed as

$$\phi(x, y, z)=\sum_{k=1}^{K}\phi_k(x, y, z)\,, \quad \cdots\cdots(29)$$

where ϕ_k is the potential induced by the k-th element. The nodes are now considered to be ordered in sequence and each node is designated by an index, i or j. Thus the value of source strength at the i-th node is denoted by σ_i. Since ϕ_k is linearly related to the source strength of the k-th element at each node, Eq. (29) is rewritten as

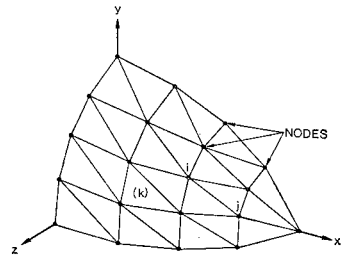

Fig. 3 Subdivision of Body Surface.

$$\phi(x, y, z)=\sum_{i=1}^{N}\sigma_i\phi_i(x, y, z)\,, \quad \cdots\cdots(30)$$

where N is the total number of the nodes and ϕ_i denotes the induced potential due to the i-th node. From the manner in which the triangular elements are formed, some elements have a vertex in common with i-th node. The potential ϕ_i is then the sum of the potentials induced by all of these elements.

We require the body to have a continuous normal vector and apply the Neumann boundary condition at a set of control points on the body surface. In this discretization process, Eq. (20) is replaced by a system of linear equations. The location of these control points may, in principle, be chosen arbitrary since there are more surface elements than unknowns. We will choose the N node points to give the following linearly independent equations with N unknown source strengths:

$$\sum_{i=1}^{N}\sigma_i \underline{\text{grad}}\,\phi_i\cdot\boldsymbol{n}_j=f_j\,, \quad j=1, \cdots N\,. \quad \cdots\cdots(31)$$

These linear equations include $2\pi\sigma_i$ that occurs in the left-hand side of Eq. (20). This term causes a complicated jump condition at a node, where the source surface is not locally flat. To exclude the jump terms from Eq. (31) we submerge the source surface slightly beneath the actual body (see **Fig. 4**). That is, submerging the source surface replaces the Fredholm integral equation of the second kind, Eq. (20), by one of the first kind. Thus it is numerically more stable to evaluate source strength in Eq. (31) at a small distance from the node rather than right at the node. Basically, selection of the depth of submergence can be determined for a given body shape by computing the normal velocities on the exact body surface, which is placed in the field of a freestream at infinity, at points other than the nodal points. **Fig. 5** displays the maximum errors of the computed normal velocity for a ellipsoid which has a diameter-length ratio of 0.5. It can be seen that an increase in the depth of submergence or the number of nodes at first leads to a decrease in the error. A further increase

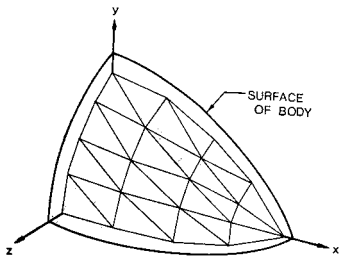

Fig. 4 Submerged Source Surface.

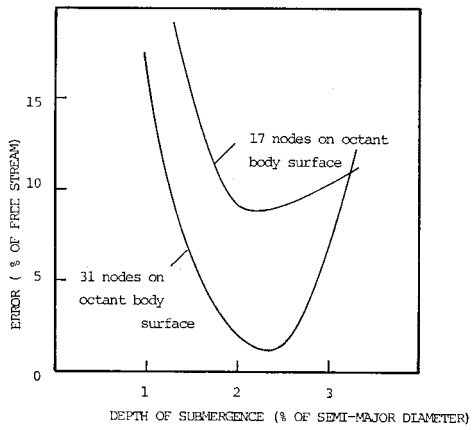

Fig. 5 Effect of Submergence of Nodes.

in the depth of submergence does not improve the accurancy. This could be caused by the fact that the approximated body surface has a blunter nose than the actual body surface. It was found that in order to obtain a well-defined solution the depth of submergence should be small compared with the dimensions of the element and that a smaller submergence should be used in the region where the body has a rapidly changing curved surface or a sharp shoulder.

5. RESULTS AND DISCUSSIONS

(1) Floating Sphere

In order to examine the efficiency of the present method, the wave forces acting on the floating semi-submerged sphere were investigated by using 36 nodes and 65 nodes (13 nodes and 20 nodes on the quarter body). The number of nodes used corresponds to 60 elements and 112 elements, respectively. The depth of submergence of the nodes was chosen to be 25 percent of

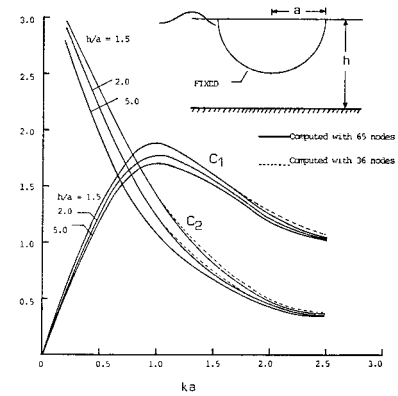

Fig. 6 Wave Force Coefficients for a Floating Sphere.

the radius. In **Fig. 6** the wave force coefficients C_1 and C_2 defined in Eq. (15) are shown as a function of ka. The results for $h/a=1.5$ and 2.0 were compared with Garrison's[7] results which were generated using 100 nodes, and the results computed with 65 nodes are identical to those from Garrison. Even the results based on 36 nodes agree well with those of Garrison.

(2) Floating Vertical Circular Cylinder

The hydrodynamic coefficients for a floating vertical circular cylinder shown in **Fig. 7** were computed using 72 nodes. The submergence of the nodes was taken small near the shoulder of the cylinder, but larger and constant for the rest of the surface. **Fig. 8** and **Fig. 9** show the wave

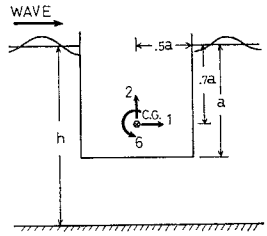

Fig. 7 Floating Vertical Circular Cylinder.

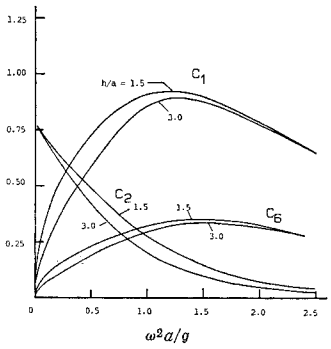

Fig. 8 Wave Force Coefficients for a Floating Vertical Circular Cylinder.

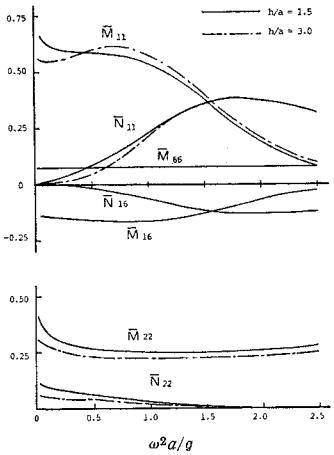

Fig. 9 Added-mass and Damping Coefficients for a Floating Vertical Circular Cylinder.

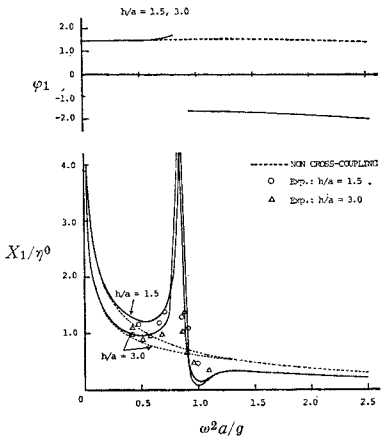

(a) Surge Response

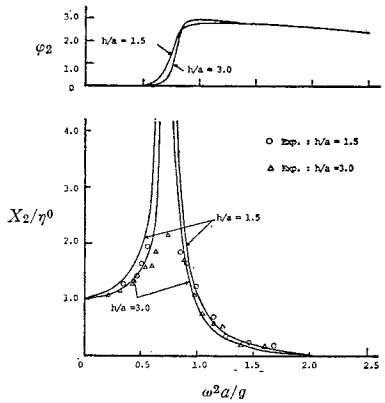

(b) Heave Response

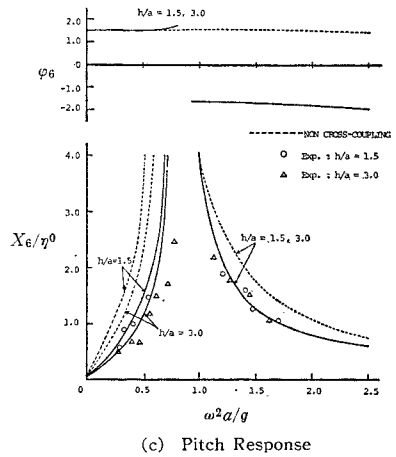

(c) Pitch Response

Fig. 10 Response of a Floating Vertical Circular Cylinder.

force or moment coefficients and the added-mass and damping coefficients, respectively. The center of gravity on the centerline was taken $0.7a$ beneath the mean waterline. In the present case the damping coefficient in pitch motion $\bar{M}_{66}$ is very small and is not shown in the figure. The surge-pitch coupling added-mass and damping coefficient, $\bar{M}_{16}$ and $\bar{N}_{16}$ are rather pronounced. Using these results the surge-heave-pitch response was evaluated by solving Eq. (17). The results of the amplitude of the motion to the amplitude of the incident wave and associated phase angle are shown in **Fig. 10**. The response resulted from omitting coupling coefficients is different in both the amplitude ratio and the phase angle. The effect of water depth is rather small for all of the cases.

The numerical results presented herein are compared with experimental data for the circular cylinder of the same specifications used for computation. For model test a circular cylinder of 10 cm in radius which is ballasted with a weight was floated in the wave tank of 20 m long, 1.75 m wide and 0.8 m deep. The motion of the cylinder was recorded with the use of the video camera of rotary-shutter type and was analyzed through a video motion analyzer. The results of the amplitude ratio are shown in **Fig. 10**. The amplitude of the incident wave is $\eta^0/a=0.25$ for the present cases. The agreement between the numerical and experimental results is fairly good except at the resonance condition. It may be noted that the general tendency of numerical and experimental results of the heave motion presented herein agrees with those of Watanabe[14], although his numerical results were generated by the method of continuation of velocity potentials and his experimental results were obtained by two-dimensional wave tank model test.

(3) Floating Semi-immersed Vertical Ellipsoid and Vertical Right Circular Cone

To see the effects of body shape the surge-heave-pitch response was evaluated for a semi-immersed vertical ellipsoid (**Fig. 11**), and for a vertical right circular cone (**Fig. 12**). The wave force, added-mass and damping coefficients as well as the resultant response for the ellipsoid are presented in **Figs. 13~15**, and those for the right circular cone in **Figs. 16~18**. For both cases, the center of gravity was assumed to lie at $0.5a$ beneath the waterline level and 65 nodes were used in the computation. The changes of the response peak and phase angle compared with the case of the vertical circular cylinder are clearly

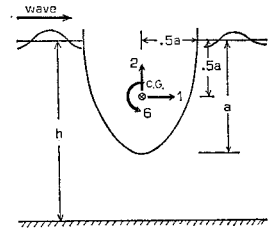

Fig. 11 Floating Vertical Semi-ellipsoid.

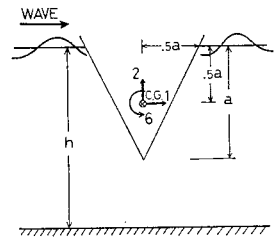

Fig. 12 Floating Vertical Right Circular Cone.

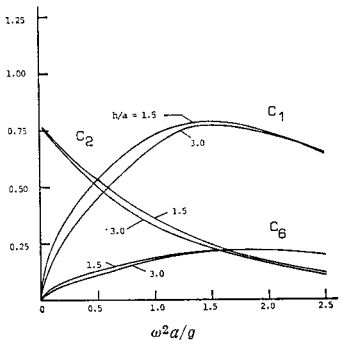

Fig. 13 Wave Force Coefficients for a Floating Vertical Semi-ellipsoid.

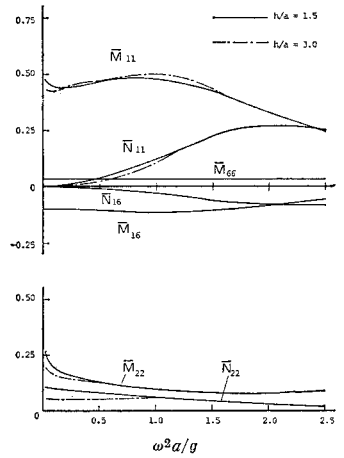

Fig. 14 Added-mass and Damping Coefficients for a Vertical Semi-ellipsoid.

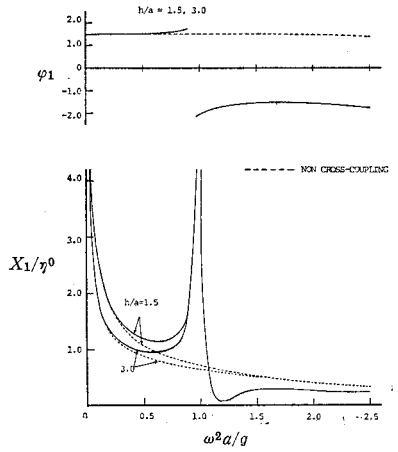

(a) Surge Response

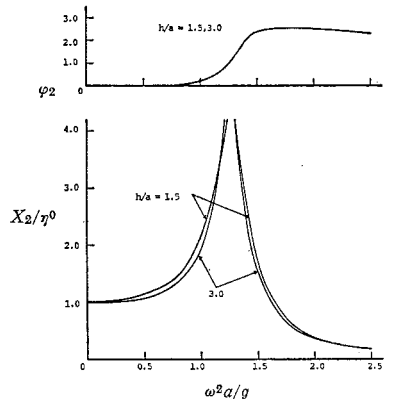

(b) Heave Response

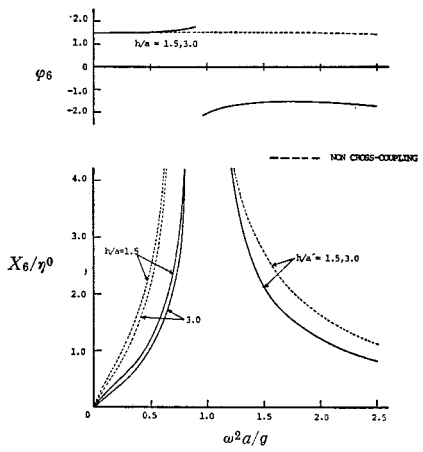

(c) Pitch Response

Fig. 15 Response of a Floating Vertical Semi-ellipsoid.

due to the changes in the bottom configuration. In particular, the right circular cone has a relatively large damping coefficient in heave, and as a result the heave response is very small. The effects of surge-pitch coupling are pronounced for the present cases.

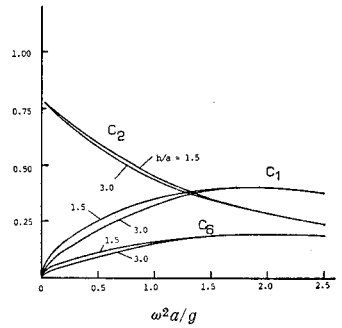

Fig. 16 Wave Force Coefficients for a Floating Vertical Right Circular Cone.

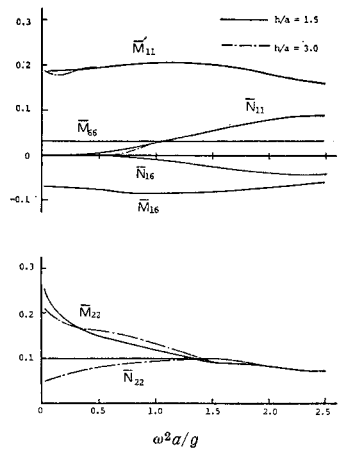

Fig. 17 Added-mass and Damping Coefficients for Floating Vertical Right Circular Cone.

6. CONCLUSIONS

The linearized boundary-valued problem for the response of a free-floating, three-dimensional body induced by wave excitation has been formulated and solved using the Green-function approach. The numerical procedure was developed utilizing a linear variation of source density and the submergence of the source surface, which are well-suited for most practical ocean structures.

The numerical results for the bodies having a relatively large draft indicate strong surge-pitch cross-coupling effects for both surge and pitch response. The limited comparisons with experimental data appear to be in good agreement.

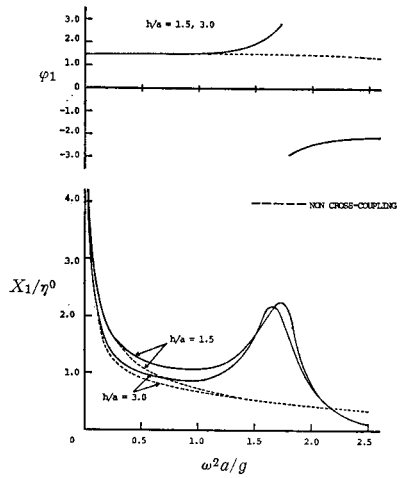

(a) Surge Response

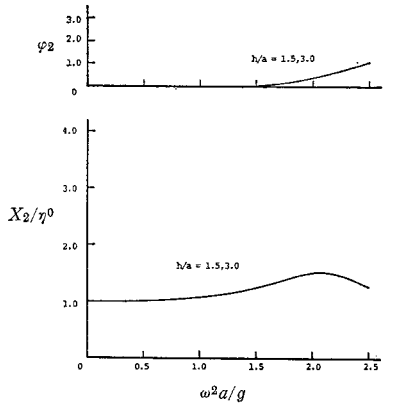

(b) Heave Response

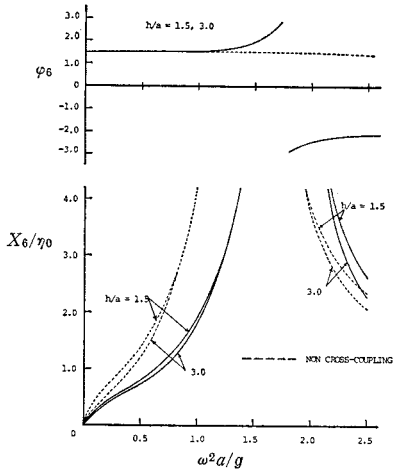

(c) Pitch Response

Fig. 18 Response of a Floating Vertical Right Circular Cone.

7. ACKNOWLEDGEMENT

A portion of this paper is based on the author's Ph. D. thesis submitted to the University of California, Berkeley. The author wishes to express his sincere gratitude to Professors Robert L. Wiegel and William C. Webster for providing the necessary advice and guidance. Special thanks are extended to the members of Editorial Committee for their most helpful suggestions.

8. APPENDIX: THE POTENTIAL AND VELOCITY VECTOR FUNCTIONS INDUCED BY A TRIANGULAR ELEMENT

We introduce the following notations:

$$
\begin{aligned}
&c=(\hat{a}^2+\hat{b}^2)^{1/2}, \quad e=(\hat{d}^2+\hat{b}^2)^{1/2},\\
&r_a=[(\hat{x}-\hat{a})^2+\hat{y}^2+\hat{z}^2]^{1/2},\\
&r_b=[(\hat{x}^2+(\hat{b}-\hat{y})^2+\hat{z}^2)]^{1/2},\\
&r_d=[(\hat{x}-\hat{d})^2+\hat{y}^2+\hat{z}^2]^{1/2}\\
&\hat{\rho}=\hat{b}\hat{x}+\hat{a}\hat{y}-\hat{a}\hat{b}, \quad \rho_a=\hat{a}\hat{x}-\hat{b}\hat{y}-\hat{a}^2,\\
&\rho_b=\hat{a}\hat{x}-\hat{b}\hat{y}+\hat{b}^2, \quad \bar{\rho}=\hat{b}\hat{x}+\hat{d}\hat{y}-\hat{d}\hat{b},\\
&\bar{\rho}_d=\hat{d}\hat{x}-\hat{b}\hat{y}-\hat{d}^2, \quad \bar{\rho}_b=\hat{d}\hat{x}-\hat{b}\hat{y}+\hat{b}^2,\\
&I_{ad}=In[(r_a-(\hat{x}-\hat{a}))/(r_d-(\hat{x}-\hat{d}))],\\
&I_{ab}=In[(cr_a+\rho_a)/(cr_b+\rho_b)],\\
&I_{db}=In[(er_d+\bar{\rho}_d)/(er_b+\bar{\rho}_b)],\\
&T=-\tan^{-1}[(\hat{a}r_b{}^2-\hat{x}\rho_b)/\hat{z}\hat{b}r_b]\\
&\quad+\tan^{-1}[(\hat{a}r_a{}^2-(\hat{x}-\hat{a})\rho_a)/\hat{z}\hat{b}r_a]\\
&\quad+\tan^{-1}[(\hat{d}r_b{}^2-\hat{x}\bar{\rho}_b/\hat{z}\hat{b}r_b]\\
&\quad-\tan^{-1}[(\hat{d}r_d{}^2-(\hat{x}-\hat{d})\bar{\rho}_d)/\hat{z}\hat{b}r_d].
\end{aligned}
\qquad \cdots\cdots\cdots\cdots\cdots\cdots\text{(A. 1)}
$$

The potential functions $\phi_a{}^r$, $\phi_b{}^r$ and $\phi_d{}^r$ are given by

$$
\begin{aligned}
\phi_a{}^r=&[2\bar{\rho}\hat{z}T+\hat{d}R_{ad}+(\hat{b}^2+\hat{a}\hat{d})F_{ab}/c^2-F_{ab}\\
&+(2\hat{\rho}\bar{\rho}-(\hat{b}^2+\hat{a}\hat{d})(\hat{z}^2+\hat{\rho}^2/c^2))I_{ab}/c\\
&+e(\hat{z}^2-\bar{\rho}^2/e^2)I_{ab}+(2\hat{y}\hat{\rho}\\
&-\hat{d}(\hat{y}^2+\hat{z}^2))I_{ad}]/2\hat{b}(\hat{a}-\hat{d}), \quad \cdots\cdots\text{(A. 2)}
\end{aligned}
$$

$$
\begin{aligned}
\phi_b{}^r=&[2\hat{y}\hat{z}T+R_{ad}+\hat{a}F_{ab}/c^2-\hat{d}F_{db}/e^2+(2\hat{y}\hat{\rho}\\
&-\hat{a}(\hat{z}^2+\hat{\rho}^2/c^2))I_{ab}/c+(\hat{y}^2+\hat{z}^2)I_{ad}\\
&-(2\hat{y}\bar{\rho}-\hat{d}(\hat{z}^2+\bar{\rho}^2/e^2))I_{db}/e]/2\hat{b}, \quad \cdots\cdots\text{(A. 3)}
\end{aligned}
$$

and

$$
\begin{aligned}
\phi_d{}^r=&[-2\hat{\rho}\hat{z}T-\hat{a}R_{ad}+(\hat{b}^2+\hat{a}\hat{d})F_{db}/e^2-F_{ab}\\
&+(2\hat{\rho}\bar{\rho}-(\hat{b}^2+\hat{a}\hat{d})(\hat{z}^2+\bar{\rho}^2/e^2))I_{db}/e\\
&+c(\hat{z}^2-\hat{\rho}^2/c^2)I_{ab}-(2\hat{y}\hat{\rho}\\
&-\hat{a}(\hat{y}^2+\hat{z}^2))I_{ad}]/2\hat{b}(\hat{a}-\hat{d}), \quad \cdots\cdots\cdots\text{(A. 4)}
\end{aligned}
$$

where

$$R_{ad}=r_a(\hat{x}-\hat{a})-r_a(\hat{x}-\hat{d}),$$
$$F_{ab}=\rho_b r_b-\rho_a r_a,$$
$$F_{db}=\bar{\rho}_b r_b-\bar{\rho}_d r_d.$$

The expressions for the velocity vector functions $\boldsymbol{v}^r=(u^r, v^r, w^r)$ are

$$\begin{aligned}u^r=&\sigma_a[(\hat{y}I_{ad}+\hat{z}T)/(\hat{a}-\hat{d})-\hat{b}(r_a-r_b)/c^2\\&+(\hat{\rho}/c(\hat{a}-\hat{d})+\hat{b}\rho_b/c^3)I_{ab}-\rho I_{db}/e(\hat{a}-\hat{d})]\\&+\rho_b[\hat{b}(r_a-r_b)/c^2+\hat{b}(r_b-r_d)/e^2\\&-\hat{b}(\rho_a I_{ab}/c^3-\bar{\rho}_d I_{ab}/e^3)]+\sigma_d[-(\hat{y}I_{ad}\\&+\hat{z}T)/(\hat{a}-\hat{d})-\hat{b}(r_b-r_d)/e^2+(\bar{\rho}/e(\hat{a}-\hat{d})\\&-\hat{b}\bar{\rho}_b/e^3)I_{db}-\hat{\rho}I_{db}/c(\hat{a}-\hat{d})|,\end{aligned}\quad\cdots\cdots\cdots\cdots\cdots\cdots\text{(A. 5)}$$

$$\begin{aligned}v^r=&\sigma_a[(\bar{\rho}I_{ad}+\hat{d}\hat{z}T)/\hat{b}(\hat{a}-\hat{d})-\hat{a}(r_a-r_b)/c^2\\&+(r_a-r_d)/(\hat{a}-\hat{d})+(\hat{a}\rho_b/c^3+\hat{d}\hat{\rho}/\hat{b}\hat{c}(\hat{a}-\hat{d}))I_{ad}\\&-\hat{d}\hat{\rho}I_{db}/\hat{b}e(\hat{a}-\hat{d})]+\sigma_b[(\hat{y}I_{db}+\hat{z}T)/\hat{b}\\&+\hat{d}(r_b-r_d)/e^2+\hat{a}(r_a-r_b)/c^2+(\hat{b}\hat{\rho}/c^3\\&+\hat{a}\hat{y}/\hat{b}\hat{c})I_{ab}-(\hat{b}\bar{\rho}/e^3+\hat{d}\hat{y}/\hat{b}e)I_{db}]\\&+\sigma_d[-(\hat{\rho}I_{ad}+\hat{a}\hat{z}T)/\hat{b}(\hat{a}-\hat{d})\\&-\hat{d}(r_b-r_d)-(r_a-r_d)/(\hat{a}-\hat{d})-(\hat{d}\bar{\rho}_b/e^3\\&-\hat{a}\bar{\rho}/\hat{b}e(\hat{a}-\hat{d}))I_{db}-\hat{a}\hat{\rho}I_{db}/\hat{b}c(\hat{a}-\hat{d})],\end{aligned}\quad\cdots\cdots\cdots\cdots\cdots\cdots\text{(A. 6)}$$

and

$$\begin{aligned}w^r=&\sigma_a[\bar{\rho}T-(\hat{a}\hat{d}+\hat{c}^2)\hat{z}I_{db}/c+e\hat{z}I_{db}\\&-\hat{d}\hat{z}I_{ad}]/\hat{b}(\hat{a}-\hat{d})+\sigma_b[\hat{y}T-\hat{a}\hat{z}I_{db}/c\\&+\hat{d}\hat{z}_{db}/e-\hat{z}I_{ad}]/\hat{b}+\sigma_d[-\hat{\rho}T-(\hat{a}\hat{d}+\hat{b}^2)\hat{z}I_{ba}/e\\&+c\hat{z}I_{ab}+\hat{a}\hat{z}I_{ad}].\end{aligned}\quad\cdots\cdots\cdots\cdots\cdots\cdots\text{(A. 7)}$$

REFERENCES

1) Black, J. L., C. C. Mei and M. C. G. Bray: Radiation and scattering of water waves by rigid bodies, J. Fluid Mech., Vol. 10, pp. 451–472, 1971.
2) Bai, K. J.: A variational method in potential flows with a free surface, Univ. of Calif., Berkeley, College of Engineering, Rep. No. NA72-2, 1972.
3) Yeung, R. W.: A singularity-distribution method for free-surface flow problems with an oscillating body, Univ. of Calif., Berkeley, College of Engineering, Rep. No. NA73-6, 1972.
4) Ijima, T., C. R. Chou and Y. Yumura: Scattering of waves by permeable and impermeable breakwater of arbitrary shape, Proc. of JSCE, No. 255, pp. 31–42, May, 1974, (in Japanese).
5) Garrison, C. J. and V. Seetharama Rao: Interaction of waves with submerged objects, J. Waterways and Harbors Div., Vol. 97, No. WW2, pp. 259–277, 1971.
6) Garrison, C. J. and R. Y. Chow: Wave forces on submerged bodies, J. Waterways and Harbors Div., Vol. 98, No. WW3, pp. 375–392, 1972.
7) Garrison, C. J.: Hydrodynamics of large objects in the sea-Part II: motion of free-floating bodies, J. Hydronautics, Vol. 9, No. 2, pp. 58–63, 1975
8) Hino, M. and Y. Miyanaga: Wave force and scattering by Green's function method and imaginary plate-load approximation, Proc. of JSCE, No. 237, pp. 51–62, May, 1975, (in Japanese).
9) Wehausen, J. V.: The motion of floating bodies, Ann. Rev. Fluid Mech., Vol. 3, pp. 237–268, 1971.
10) John, F.: On the motion of floating bodies II, Comm. Pure Appl. Math., Vol. 3, pp. 45–101, 1950.
11) Wehausen, J. V. and E. V. Laitone: Surface waves, Encyclopedia of Physics, Vol. 9, Springer-Verlag, Berlin, pp. 475–479, 1960.
12) Webster, W. C.: The flow about arbitrary three-dimensional smooth bodies, J. Ship Res., Vol. 19, No. 4, pp. 206–218, 1975.
13) Kioka, W.: A Green-function method for wave interaction with a submerged body, Univ. of Calif., Berkeley, College of Engineering, Rep. No. UCB/EERC-80/11, 1980.
14) Watanabe, A.: Motion of floating vertical circular cylinder induced by wave excitation, Proc. of 25th Japanese Conference on Coastal Engineering, p. 380, 1978, (in Japanese).

(*Received November 18, 1980*)